13. Zaránd, G., Brataas, A. & Goldhaber-Gordon, D. Kondo effect and spin filtering in triangular artificial atoms. *Solid State Commun.* **126,** 463–466 (2003).
14. López, R. *et al.* Probing spin and orbital Kondo effects with a mesoscopic interferometer. Preprint available at ⟨http://xxx.lanl.gov/abs/cond-mat/0402361⟩.
15. Sasaki, S., Amaha, S., Asakawa, N., Eto, M. & Tarucha, S. Enhanced Kondo effect via tuned orbital degeneracy in a spin $\frac{1}{2}$ artificial atom. *Phys. Rev. Lett.* **93,** 017205 (2004).
16. Dresselhaus, M. S., Dresselhaus, G. & Eklund, P. C. *Science of Fullerenes and Carbon Nanotubes* (Academic, San Diego, 1996).
17. Minot, E., Yaish, Y., Sazonova, V. & McEuen, P. L. Determination of electron orbital magnetic moments in carbon nanotubes. *Nature* **428,** 536–539 (2004).
18. Ajiki, H. & Ando, T. Electronic states of carbon nanotubes. *J. Phys. Soc. Jpn.* **62,** 1255–1266 (1993).
19. Zaric, S. *et al.* Optical signatures of the Aharonov–Bohm phase in single-walled carbon nanotubes. *Science* **304,** 1129–1131 (2004).
20. Coskun, U. C., Wei, T.-C., Vishveshwara, S., Goldbart, P. M. & Bezryadin, A. *h*/*e* magnetic flux modulation of the energy gap in nanotube quantum dots. *Science* **304,** 1132–1134 (2004).
21. Jarillo-Herrero, P. *et al.* Electronic transport spectroscopy of carbon nanotubes in a magnetic field. Preprint available at ⟨http://xxx.lanl.gov/cond-mat/0411440⟩.
22. Liang, W., Bockrath, M. & Park, H. Shell filling and exchange coupling in single-walled carbon nanotubes. *Phys. Rev. Lett.* **88,** 126801 (2002).
23. De Franceschi, S. *et al.* Electron cotunneling in a semiconductor quantum dot. *Phys. Rev. Lett.* **86,** 878–881 (2001).
24. Paaske, J., Rosch, A. & Wölfle, P. Nonequilibrium transport through a Kondo dot in a magnetic field: perturbation theory. *Phys. Rev. B* **69,** 155330 (2004).
25. Pasupathy, A. N. *et al.* The Kondo effect in the presence of ferromagnetism. *Science* **306,** 86–89 (2004).
26. Costi, T. A. Kondo effect in a magnetic field and the magnetoresistivity of Kondo alloys. *Phys. Rev. Lett.* **85,** 1504–1507 (2000).
27. Sasaki, S. *et al.* Kondo effect in an integer-spin quantum dot. *Nature* **405,** 764–767 (2000).
28. Choi, M.-S., López, R. & Aguado, R. SU(4) Kondo effect in carbon nanotubes. *Phys. Rev. Lett.* (submitted).
29. Mann, D., Javey, A., Kong, J., Wang, Q. & Dai, H. J. Ballistic transport in metallic nanotubes with reliable Pd ohmic contacts. *Nano Lett.* **3,** 1541–1544 (2003).
30. Bonet, E., Deshmukh, M. M. & Ralph, D. C. Solving rate equations for electron tunneling via discrete quantum states. *Phys. Rev. B* **65,** 045317 (2002).

Supplementary Information accompanies the paper on **www.nature.com/nature**.

Acknowledgements We thank G. Zaránd, R. Aguado and J. Martinek for discussions. Financial support was obtained from the Japanese Solution Oriented Research for Science and Technology (SORST) program and the Dutch Fundamenteel Onderzoek der Materie (FOM).

Competing interests statement The authors declare that they have no competing financial interests.

Correspondence and requests for materials should be addressed to P.J. (pablo@qt.tn.tudelft.nl).

Compact, stable and efficient all-fibre gas cells using hollow-core photonic crystal fibres

F. Benabid, F. Couny, J. C. Knight, T. A. Birks & P. St J. Russell

Photonics and Photonic Materials Group, Department of Physics, University of Bath, Bath BA2 7AY, UK

Gas-phase materials are used in a variety of laser-based applications—for example, in high-precision frequency measurement[1,2], quantum optics and nonlinear optics[3,4]. Their full potential has however not been realized because of the lack of a suitable technology for creating gas cells that can guide light over long lengths in a single transverse mode while still offering a high level of integration in a practical and compact set-up or device. As a result, solid-phase materials are still often favoured, even when their performance compares unfavourably with gas-phase systems. Here we report the development of all-fibre gas cells that meet these challenges. Our structures are based on gas-filled hollow-core photonic crystal fibres, in which we have recently demonstrated substantially enhanced stimulated Raman scattering[5,6], and which exhibit high performance, excellent long-term pressure stability and ease of use. To illustrate the practical potential of these structures, we report two different devices: a hydrogen-filled cell for efficient generation of rotational Raman scattering using only quasi-continuous-wave laser pulses; and acetylene-filled cells, which we use for absolute frequency-locking of diode lasers with very high signal-to-noise ratios. The stable performance of these compact gas-phase devices could permit, for example, gas-phase laser devices incorporated in a 'credit card' or even in a laser pointer.

Our all-fibre gas cells consist of hollow-core photonic crystal fibre (HC-PCF) filled with gas and spliced hermetically at both ends to standard single-mode optical fibre (SMF) (Fig. 1a, d). These novel devices have no bulk-optics components, and may be used with a wide range of commercially available optical fibre components (such as couplers, filters, mirrors and lasers). Moreover, the use of HC-PCF in which light is guided in a single transverse mode by means of a photonic bandgap created in the 'photonic crystal' cladding[7] greatly increases the efficiency of these laser–gas devices[5,6].

The high air-filling fraction of the HC-PCFs (which are formed by a network of glass webs typically just a few hundred nanometres thick) makes it very challenging to fusion-splice these fibres without collapsing and deforming the microstructure, which would give a high insertion loss. It is also important to avoid contaminating the PCF with solid deposits and water. Nevertheless, after some practice, routine splicing of HC-PCF to SMF was achieved with a typical loss of 1–2 dB. We estimate that a perfect splicing procedure using our fibres would yield a loss of 0.6–0.8 dB. Of this, 0.15 dB arises from the refractive index mismatch between the fibre cores, and is therefore fundamental. The rest is due to modal field mismatch, which we estimate by the butt-joint approximation[8] to be 0.4–0.6 dB. The discrepancy between estimated and achieved splice losses is linked to the formation of a recess in the end face of the HC-PCF when heated in the splicer (Fig. 1b). We believe this results from the action of surface tension along the many glass–air interfaces within the holey structure, the viscosity of which offers much less resistance to deformation than the solid glass in the outer cladding of the fibre. The mechanical strength of the splices is

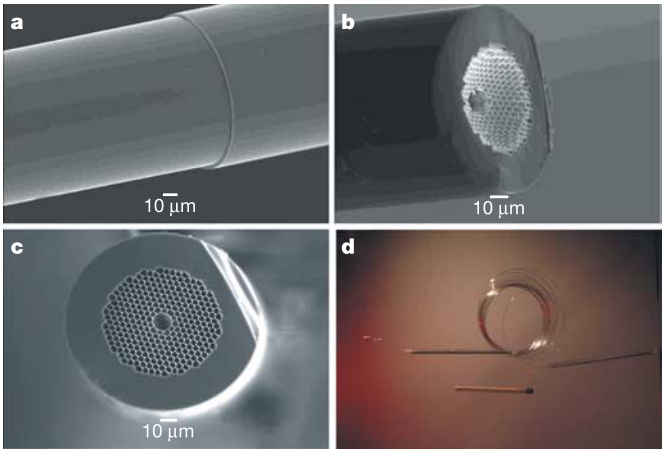

Figure 1 HC-PCF-based gas-cell assembly. **a**–**c**, Images obtained using a scanning electron microscope. **a**, Side view of a 1,550 nm HC-PCF (the narrower fibre) spliced to an SMF. **b**, End view of an HC-PCF cleaved at the junction of the splice. The recess, which creates an air gap of a few tens of micrometres between the fibre cores, is due to the action of surface tension during fusion. **c**, View of the same piece of HC-PCF as in **a** and **b** but cleaved a few millimetres from the splice, showing clearly the preservation of the microstructural integrity. **d**, Photograph of a 5-m-long hydrogen-filled HC-PCF gas cell, showing its size compared to that of a match.

equivalent to a gas pressure of 80 bar—of crucial importance for containment of gases at high pressure.

To form a gas cell, one end of the HC-PCF was fusion-spliced to SMF (see Methods). The HC-PCF was then evacuated for several hours (depending on the length) from the remaining open end to a pressure of ~1 μbar, before being backfilled with the desired gas as described in our previous work[5]. Finally, once the desired fill pressure was achieved, the second end of the HC-PCF was spliced to SMF in the same way as the first splice. Using this procedure, several hydrogen cells and several acetylene cells (Fig. 1d) were produced, with gas fill pressures (before splicing) ranging from 6 mbar to 500 mbar for the former, and from 5 bar to 10 bar for the latter. The acetylene cells were made from HC-PCF with a guidance band centred at 1,550 nm and a loss of 18 dB km^{-1}. The hydrogen cells were made from the same material with a guidance band centred at 1,064 nm and a transmission loss of 60–70 dB km^{-1}. In all cases, the splice losses were 1–2 dB. Although both gases were highly flammable, no damage to the fibre was apparent during the second splice.

In stimulated Raman scattering (SRS), photons of the incident 'pump' laser beam are converted to photons of lower frequency through interactions with molecules in an excited (vibrational or rotational) state. This conversion process becomes highly efficient in HC-PCF, where high intensities and long interaction lengths are available. This has removed the need for powerful lasers, making SRS an ideal technique for efficient laser-frequency conversion and high-resolution spectroscopy. Here we use an experimental set-up (similar to one described previously[5,6]) to generate rotational SRS in a 5-m-long in-line hydrogen gas cell with quasi-continuous-wave pulses. The pump source is a *Q*-switched Nd:YVO_4 laser at 1,047 nm, with a pulse width tunable in the range 6–50 ns. In all the hydrogen cells we made, we were able to generate SRS with pump pulses as long as 35 ns at peak powers of only 100–180 W. Figure 2a and b shows the typical measured spectra at day 1 and day 37, respectively, when a pulse of 13 ns duration and peak power ~200 W is launched into a hydrogen cell with a fill pressure of ~6 bar and a splice loss of 1.6 dB and 2 dB for the input and output splices, respectively. The richness of the generated spectrum at such low peak powers illustrates the extreme effectiveness of the gas cell as a Raman converter.

The lifetime of such a cell has been assessed by carrying out threshold measurements on a daily basis on our hydrogen cells (see Methods). Figure 2c shows the evolution with time of the measured threshold peak power (7-ns pulses). The average measured threshold was ~98 ± 14 W over a period exceeding 1 month. The measured spectra are identical within the uncertainty of our measurement, indicating good stability of the gas cell over the measurement period. In principle, with a strong seal, the hydrogen will escape only via diffusion through the silica, which in our case (isothermal conditions at room temperature and for a fill pressure of ~6 bar) would yield a leakage rate of less than 0.001 mol yr^{-1}

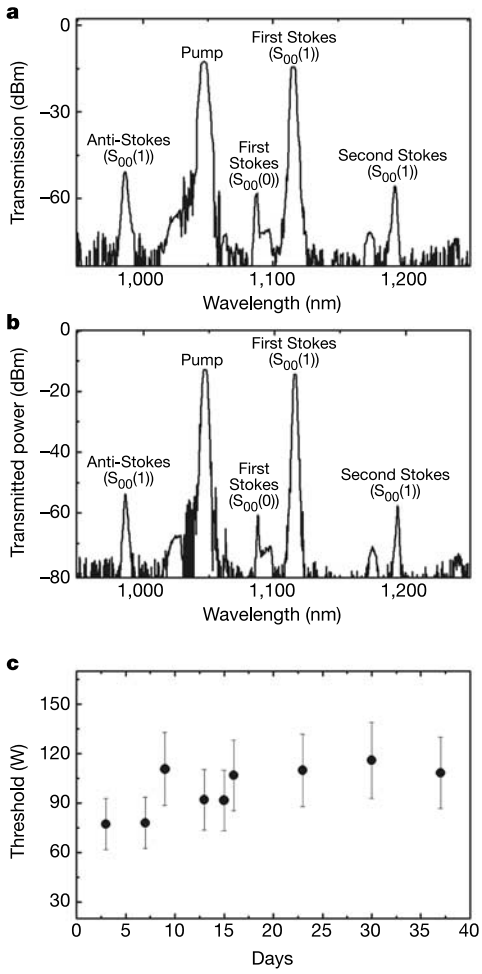

Figure 2 The SRS spectrum generated by a hydrogen-filled HC-PCF gas cell, and its behaviour as a function of time. **a**, **b**, Rotational SRS spectra generated using a 13-ns pulse with a peak power in the range of 150–200 W at day 1 (**a**) and day 37 (**b**). For both traces, in addition to the pump line, the spectrum contains three lines from the rotational transition $S_{00}(1)$ in ortho-hydrogen; the first Stokes (~1,115 nm), the second Stokes (~1,194 nm), and finally the first anti-Stokes at ~986 nm, which is the product of wave mixing between the pump and the first Stokes. Also, the spectrum exhibits a peak at ~1,087 nm, which corresponds to the first Stokes line of the much weaker Raman transition, $S_{00}(0)$, from the para-hydrogen present (~30%) in normal hydrogen gas. **c**, The variation with time of the peak power of the pump threshold for the generation of the first Stokes of $S_{00}(1)$. The error bars indicate the standard error on the threshold measurement.

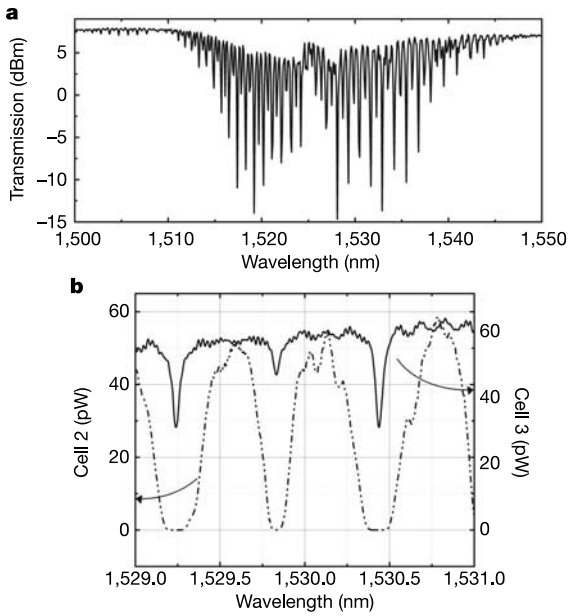

Figure 3 Transmission spectra of acetylene-filled HC-PCF gas cells. **a**, Transmission spectrum through a 1-m-long HC-PCF-based $^{12}C_2H_2$ cell. The spectrum exhibits more than 50 strong lines, thereby providing a wide grid of frequency references. **b**, Close-up view of the transmission spectrum of cell 2 (fill pressure ~200 mbar) and cell 3 (fill pressure ~6 mbar) with a resolution of 0.01 nm around 1,530 nm. The linewidths in cell 3 are Doppler limited.

(ref. 9), suggesting that the lifetime of the cell could extend to several decades.

Accurate stabilization of laser frequency is essential in many fields[1,2], such as high-resolution spectroscopy, measurements of fundamental physical constants[10,11], atomic physics and optical telecommunications; in all these cases, there is a pressing need for wavelength accuracy and stability to reduce the spacing between the channels, and increase their number, in wavelength division multiplexed systems. This can be achieved by locking the laser frequency to an optical frequency reference—usually an ensemble of atoms or molecules with a narrow absorption line. The performance of the stabilization system is limited by the fractional frequency fluctuations. One needs a high quality factor, Q ($Q=\nu/\Delta\nu$, where ν is the carrier frequency and $\Delta\nu$ is the linewidth of the reference line), and a high signal-to-noise ratio, which is in turn determined by the stabilization detection scheme and the interaction length between the light and the absorber. The long interaction lengths offered by HC-PCF[5,6] permit large enhancements in signal-to-noise ratio.

Acetylene is suitable for the optical communications wavelength range[12], offering a comb of stable and regularly spaced overtone absorptions in the vicinity of 1.55 μm. It exhibits Doppler-free saturation linewidths of less than 1 MHz (ref. 13) and is remarkably insensitive to external perturbations[14]. Figure 3a shows the typical transmitted spectrum of a broad LED (light-emitting-diode) light source through a 1-m-long HC-PCF-based acetylene cell. Figure 3b shows a more detailed spectrum around the 1,530.5-nm line transmitted through two cells (labelled cell 3 and cell 2) of the same length (1 m) but containing acetylene at different pressures (~6 mbar for cell 2 and ~200 mbar for cell 3). Most of the strong lines exhibit more than 90% absorbance.

For illustrative purposes, an all-fibre frequency stabilization system was built and tested (Fig. 4a). A simple side-locking technique was used to lock to one of the shoulders of a selected absorption line[15]. This approach, though it does not offer the best performance, has the merit of being simple and modulation-free. The set-up consisted of a tunable extended cavity diode laser (ECDL) source, an isolator, two couplers and a length of acetylene-filled HC-PCF. The laser output, after passing the isolator, is split into three parts using two fused taper couplers. The first (the locking beam) passes through the gas cell (cell 3) and is detected. The second (the reference beam) is monitored at an identical detector. The reference and locking signals are sent to a difference amplifier before being fed to a locking circuit based on ref. 15. Before switching on the control loop, the wavelength of the laser is tuned to the desired absorption line. To avoid possible artefacts in the control system[16], it is important to have an independent means of testing (discriminating) the absolute frequency. This was achieved by passing the third (out-of-loop) part of the laser beam through a second HC-PCF acetylene cell ('monitor cell' in Fig. 4a). This resulted in a frequency stabilization and testing system that was completely fibre-based—to our knowledge, the first time this has been shown. Using this system, we were able to lock the laser to different acetylene absorption lines.

This is illustrated in Fig. 4b and c. Figure 4b shows the detected transmission at 1,530.43 nm (P9 absorption[14]) from the locking and monitor cells as the laser frequency is swept through 2 GHz. Figure 4c shows the frequency fluctuations of the laser when it is free

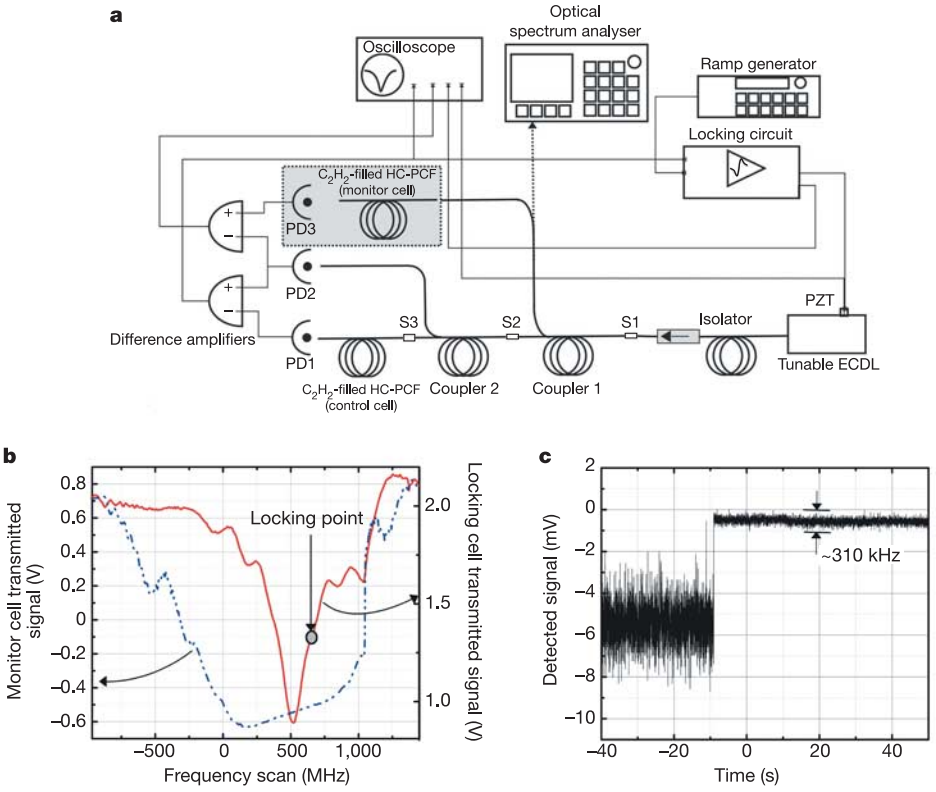

Figure 4 All-fibre frequency stabilization and discrimination system using acetylene (C_2H_2)-filled cells. **a**, Schematic representation of the frequency-locking set-up. PD, photodetector; S, splice; ECDL, extended cavity diode laser. PZT, piezo-electrical transducer. **b**, The red solid curve shows the detected absorption peaks (P9 line) after transmission through the control cell, and the blue dot-dash curve those detected after the monitor cell. The asymmetric shape of the P9 absorption peak measured at the monitor cell is caused by weak excited state absorption lines[17] and the etalon effect of the gas cell, and is consistent with the trace from the optical spectrum analyser. The locking point represents the frequency at which the laser is locked. **c**, The frequency fluctuations of the laser when free running (left-hand part of the trace) and when locked, as monitored by the out-of-loop acetylene cell. The frequency fluctuations of the laser when the locking loop is closed exhibit a maximum r.m.s. frequency deviation of ~310 kHz.

running and when the locking loop is closed. The closed-loop frequency fluctuations exhibit a root-mean-square (r.m.s.) frequency deviation of ~310 kHz over a 1-min integration time. The residual noise exhibits a white noise spectrum with an Allan variance of $3 \times 10^{-11}/\tau^{1/2}$ for an averaging time of $1\,\mathrm{s} \leq \tau \leq 25.6\,\mathrm{s}$, and is limited by the electronic noise of our detection system (PD3 in Fig. 4a).

A straightforward improvement would be to use a saturable absorption line (which can have a linewidth as narrow as 1 MHz; ref. 13) as a reference. The improved signal-to-noise ratio in HC-PCF also makes overtone absorptions in the visible and near-infrared (for example, P11 of $^{12}C_2H_2$ at 790.703 nm) accessible to laser frequency metrology. To test for gas leakage, the pressure-dependent linewidth of the P9 acetylene absorption was monitored daily over two months. The results gave an average value of ~468 MHz with a standard deviation of 30 MHz, that is, the linewidth is consistent with the Doppler limited value and was constant within experimental error, indicating no measurable leakage of gas.

In conclusion, all-fibre, ultra-compact, high performance, easy-to-use and unconditionally stable gas-laser devices have been reported. The commercial availability of a wide range of all-fibre components (for example, lasers, phase modulators, power attenuators, isolators, Bragg gratings and beam-splitters) makes complex systems easy to design and construct. It is now possible to imagine miniature laser–gas devices, occupying a tiny volume and containing minute amounts of gas, with everyday applications in fields such as the colour conversion of laser light (perhaps using a built-in diode pump laser), and the measurement and stabilization of laser frequency. The unique features of HC-PCFs make these gas–laser devices extremely efficient, and their impact in many laser-related fields is likely to be deep and lasting. □

Methods

Splicing procedure

Fusion-splicing was carried out using a commercial filament-based splicer (Vytran FFS-2000-PM). In this splicer, the splicing region is continuously purged by argon gas to stop the filament burning. This prevents contamination of the splice by solid deposits and water condensation, and also prevents combustion of flammable gases such as hydrogen and acetylene. For high fill pressures, the splice could be consolidated using heat-curable glue.

Threshold measurements

The energy threshold measurement for the generation of the first Stokes line $S_{00}(1)$ was carried out in the following manner. The input power was varied by manual rotation of a half-wave plate, and the output light was collected and fed to an optical spectrum analyser and power detectors. The detected signal at the Stokes wavelength was monitored as the input power was increased up to a point where the Stokes signal emerged abruptly from the noise on the optical spectrum analyser. With this technique, we found a relative uncertainty varying between 40% and 70%.

Received 3 November 2004; accepted 6 January 2005; doi:10.1038/nature03349.

1. Luiten, A. N. (ed.) *Frequency Measurement and Control* (Springer, Berlin, 2001).
2. Hall, J. L. Frequency stabilized lasers—a parochial review. *Proc. SPIE* **1837,** 2–15 (1992).
3. Hentschel, M. *et al.* Attosecond metrology. *Nature* **414,** 509–513 (2001).
4. Steinmeyer, G., Sutter, D. H., Gallmann, L., Matuschek, N. & Keller, U. Frontiers in ultrashort pulse generation: Pushing the limits in linear and nonlinear optics. *Science* **286,** 1507–1512 (1999).
5. Benabid, F., Knight, J. C., Antonopoulos, G. & Russell, P. S. J. Stimulated Raman scattering in hydrogen-filled hollow-core photonic crystal fiber. *Science* **298,** 399–402 (2002).
6. Benabid, F., Bouwmans, G., Knight, J. C., Russell, P. S. J. & Couny, F. Ultra-high efficiency laser wavelength conversion in gas-filled hollow core photonic crystal fiber by pure stimulated rotational Raman scattering in molecular hydrogen. *Phys. Rev. Lett.* **93,** 123903 (2004).
7. Russell, P. Photonic crystal fibers. *Science* **299,** 358–362 (2003).
8. Marcuse, D. Loss analysis of single-mode fiber splices. *Bell Syst. Tech. J.* **55,** 703–718 (1977).
9. Dushman, S. *Scientific Foundations of Vacuum Technique* (John Wiley & Sons, New York, 1962).
10. Hansch, T. W. in *The Hydrogen Atom* (ed. Hansch, T. W.) 93–102 (Springer, Berlin, 1989).
11. Huber, A. *et al.* Hydrogen-deuterium 1S–2S isotope shift and the structure of the deuteron. *Phys. Rev. Lett.* **80,** 468–471 (1998).
12. Quinn, T. J. Practical realization of the definition of the metre, including recommended radiations of other optical frequency standards (2001). *Metrologia* **40,** 103–133 (2003).
13. Nakagawa, K., de Labachelerie, M., Awaji, Y. & Kourogi, M. Accurate optical frequency atlas of the 1.5 μm bands of acetylene. *J. Opt. Soc. Am. B* **13,** 2708–2714 (1996).
14. Swann, W. C. & Gilbert, S. L. Pressure-induced shift and broadening of 1510–1540-nm acetylene wavelength calibration lines. *J. Opt. Soc. Am. B* **17,** 1263–1270 (2000).
15. MacAdam, K. B., Steinbach, A. & Wieman, C. A narrow band tunable diode laser system with grating feedback, and a saturated absorption spectrometer for Cs and Rb. *Am. J. Phys.* **69,** 1098–1111 (1992).
16. Wieman, C. E. & Hollberg, L. Using diode lasers for atomic physics. *Rev. Sci. Instrum.* **62,** 1–20 (1991).
17. Onae, A. *et al.* Optical frequency link between an acetylene stabilized laser at 1542 nm and an Rb stabilized laser at 778 nm using a two-color mode-locked fiber laser. *Opt. Commun.* **183,** 181–187 (2000).

Acknowledgements The support of the UK Engineering and Physical Sciences Research Council (EPSRC) is acknowledged. F.B. thanks A. Luiten and M. Maric for discussions on frequency stabilization. F.B. is an EPSRC Advanced Research Fellow.

Competing interests statement The authors declare that they have no competing financial interests.

Correspondence and requests for materials should be addressed to F.B. (pysab@bath.ac.uk).

Obliquity pacing of the late Pleistocene glacial terminations

Peter Huybers[1] **& Carl Wunsch**[2]

[1]*Woods Hole Oceanographic Institution, Woods Hole, Massachusetts 02543, USA*
[2]*Massachusetts Institute of Technology, Cambridge, Massachusetts 02139, USA*

The 100,000-year timescale in the glacial/interglacial cycles of the late Pleistocene epoch (the past ~700,000 years) is commonly attributed to control by variations in the Earth's orbit[1]. This hypothesis has inspired models that depend on the Earth's obliquity (~40,000 yr; ~40 kyr), orbital eccentricity (~100 kyr) and precessional (~20 kyr) fluctuations[2–5], with the emphasis usually on eccentricity and precessional forcing. According to a contrasting hypothesis, the glacial cycles arise primarily because of random internal climate variability[6–8]. Taking these two perspectives together, there are currently more than thirty different models of the seven late-Pleistocene glacial cycles[9]. Here we present a statistical test of the orbital forcing hypothesis, focusing on the rapid deglaciation events known as terminations[10,11]. According to our analysis, the null hypothesis that glacial terminations are independent of obliquity can be rejected at the 5% significance level, whereas the corresponding null hypotheses for eccentricity and precession cannot be rejected. The simplest inference consistent with the test results is that the ice sheets terminated every second or third obliquity cycle at times of high obliquity, similar to the original proposal by Milankovitch[12]. We also present simple stochastic and deterministic models that describe the timing of the late-Pleistocene glacial terminations purely in terms of obliquity forcing.

To test whether the glacial variability is related to changes in Earth's astronomical configuration, we adopt a formal null-hypothesis (H_0) that glacial terminations are independent of obliquity variations, and the alternative hypothesis (H_1) that glacial terminations are paced by it. Our focus on obliquity is motivated by previous indications of nonlinear interactions between obliquity period and quasi-100-kyr glacial variability[13], but we also perform identical tests for pacing by precession and eccentricity. The test is focused on glacial terminations because their magnitude and abruptness facilitate accurate identification.

Several obstacles must be overcome to distinguish between H_0 and H_1. A major problem is the need to establish time controls on the glacial variability. Many studies estimate age by assuming a relationship between climate proxy variability and orbital